Engineering Fracture Mechanics 277 (2023) 108955

Contents lists available at ScienceDirect

Engineering Fracture Mechanics

journal homepage: www.elsevier.com/locate/engfracmech

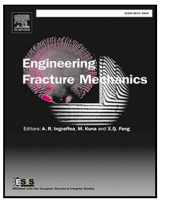

A novel, total-iterative approach to model quasi-brittle materials

J. Alfaiate [a,*], L.J. Sluys [b]

[a] CERIS, Instituto Superior Técnico, Universidade de Lisboa, Av. Rovisco Pais 1, 1049-001 Lisboa, Portugal
[b] Delft University of Technology, Department of Civil Eng. and Geosciences, P.O. Box 5048, 2600 GA Delft, The Netherlands

ARTICLE INFO

Keywords:
Total iterative approach
Iterative methods
Softening behaviour

ABSTRACT

In quasi-brittle materials, such as reinforced concrete, localisation of initially diffuse cracking evolving in localised cracking patterns consists of a numerically challenging task. With conventional iterative methods, convergence of the numerical solution scheme to model crack localisation is often difficult to obtain. On the other hand, conventional total approaches, such as the Sequentially Linear Approach, although robust, fail to approximate properly the underlying material law. In the present work, a new model is introduced, designated the Total Iterative Approach, in which the internal damage variables are updated iteratively. It is found that this approach is robust, allows for the correct approximation of the material law and is a powerful tool for the analysis of softening behaviour. Some examples are presented to illustrate the performance of the model.

1. Introduction

Softening materials, namely concrete, masonry and glass, exhibit unstable behaviour. This is due to the loss of ellipticity in the governing set of equations as well as the loss of positive definiteness of the material tangent operator, which leads to non-uniqueness or bifurcation of the numerical solution [1–4]. In continuum modelling, softening is known to give rise to pathological mesh dependence. Here, a discrete crack approach is adopted, in which the pathological mesh dependence problem is implicitly overcome. However, non-uniqueness and instability remain a major challenge for the numerical modelling of quasi-brittle materials. Iterative techniques based on the Newton–Raphson method, with or without the use of an Arc Length algorithm are usually adopted [5–8], but convergence is often difficult to achieve. Moreover, these materials exhibit several other nonlinearities, such as compressive crushing in concrete and masonry, bond–slip between substrate and internal or external reinforcement and plastic behaviour of steel reinforcement. Furthermore, in reinforced concrete, masonry and glass, a large number of cracks develop, which may lead to non-convergence with these traditional iterative techniques.

Different strategies have been studied using non-iterative methods, in the scope of both purely total and mixed incremental/total approaches. In all these strategies, based on the Sequentially Linear Approach (SLA) [9–18], the evolution of the material response is based on the enforcement of the damage state. In [19], two additional non-iterative proposals were presented, namely an Improved Total Analysis for Non-proportional Loading, as well as a Secant-incremental Approach. Both schemes were shown to overcome problems related to non-proportional loading which are associated with purely total approaches. Nevertheless, in all these Non-Iterative methods, the *correct* stiffness update is not obtained since the enforcement of increasing damage is done in a heuristic manner: damage is updated in one material point only, leading to saw-tooth load–displacement responses, as well as to possible violation of the consistency condition [19].

* Corresponding author.
E-mail address: jorge.alfaiate@tecnico.ulisboa.pt (J. Alfaiate).

https://doi.org/10.1016/j.engfracmech.2022.108955
Received 12 July 2022; Received in revised form 3 October 2022; Accepted 16 November 2022
Available online 19 November 2022

List of acronyms and symbols

IA	Incremental Approach
TA	Total Approach
TIA	Total Iterative Approach
NIEM	Non-Iterative Energy Based Method
DSDA	Discrete Strong Discontinuity Approach
MC	Mohr–Coulomb
$\mathbf{F}$	Applied force vector
Δ	increment
$\|.\|$	the norm of (.)
λ	loading factor
σ	n stress component
$\boldsymbol{\sigma}$	stress tensor
d	scalar damage variable
$\mathbf{d}$	second order damage tensor
d_n	normal damage variable component
d_s	shear damage variable component
$\boldsymbol{\varepsilon}$	strain tensor
$\mathbf{w}$	displacement jump vector
w_n	normal component of the jump displacement vector
w_s	shear component of the jump displacement vector
$\mathbf{t}$	traction vector acting at the discontinuity
t_n	normal component of the traction vector
t_n	normal traction corresponding to the maximum shear strength
t_s	shear component of the traction vector
$\mathbf{D}^{el}_{\Gamma_d}$	second order elastic constitutive tensor corresponding to discontinuity Γ_d
D^{el}_{nn}	normal diagonal component of tensor $\mathbf{D}^{el}_{\Gamma_d}$
D^{el}_{ss}	shear diagonal component of tensor $\mathbf{D}^{el}_{\Gamma_d}$
f	loading surface defined in the traction space
f_1, f_2	limit surfaces defined in the traction space
f_{t0}	initial tensile strength
f_t	tensile strength
c_0	initial cohesion: shear strength under the absence of normal traction
c	cohesion
G_F	fracture energy
G_F^{II}	fracture energy under mode-II fracture
κ	monotonic increasing function of the displacement jump components
g	loading function defined in the displacement jump space
g_n	normal damage evolution law
g_s	shear damage evolution law
ϕ	internal friction angle; diameter of reinforcement bar
ξ_n	w_n/κ_n
ξ_s	$\|w_s\|/\kappa_s$
G	c/f_t
ρ	κ_s/κ_n
C	control loading function used with the Total Iterative Approach

Alternative iterative methods have been used, such as the LATIN method [20] — LArge Time INcrement method for modelling quasi-brittle failure, or limiting the number of iterations by means of an implicit/explicit scheme, designated the IMPLEX method [21]. An incremental Sequentially Linear Analysis is also presented in [22–24], in which an iterative procedure is implemented. As in all Sequentially Linear approaches, saw-tooth load displacement responses are still obtained as well as local violation of consistency condition.

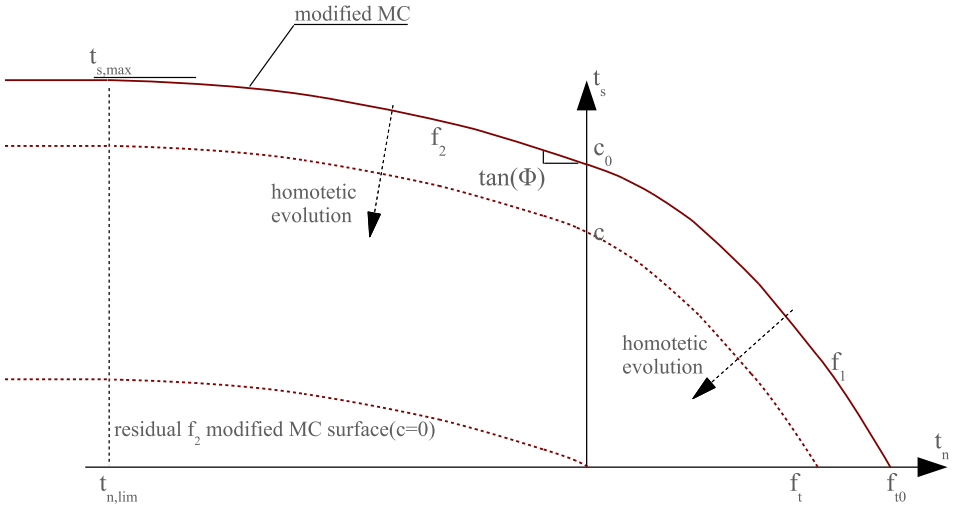

Fig. 1. Limit surface in the traction space.

In this manuscript, a new numerical method is presented, designated the Total Iterative Approach. In this method, a Total Approach is adopted since: (i) it is robust and (ii) conversely to the Incremental Approach, it allows for the evaluation of damage increase in time, under constant loading. The latter advantage is important to properly simulate the effect of corrosion, for instance. An iterative procedure is introduced to *correct* the stiffness response. This iterative procedure is also damage based, but the stiffness update is no longer heuristic; instead, the stiffness update is performed iteratively, until the Kuhn–Tucker conditions are approximately satisfied at all material points.

In the next Section, a mixed-mode strong discontinuity damage model [25] is briefly reviewed, allowing for the description of the numerical algorithms in a generalised platform. The new proposed numerical model is compared to the Incremental Approach and to the Total Approach. This is why these two formulations are reviewed in Sections 3 and 4, respectively. The new model is introduced in Section 6. Several examples are presented to illustrate the performance of the model, involving: bending, bond–slip, use of both interfaces and embedded discontinuities to model softening, snap-back and reinforced concrete.

2. A mixed-mode damage model for cohesive fracture

All iterative and non-iterative methods presented are based on damage modelling. Thus, the material models used with these methods should provide the evaluation of damage as a means of following nonlinear behaviour, both under hardening and softening. In this Section a general mixed-mode damage model presented in [25–27] is briefly reviewed. Both non-dilatant and dilatant cases are considered.

Similar to the works presented in [28–31], the model is developed within the scope of a discrete crack (or strong discontinuity) approach, defining the relationship between discontinuity displacement jumps and tractions. The damage evolution law is driven by the traction field and the limit surface in the traction space shown in Fig. 1 is defined. In a general, non-isotropic, discrete damage framework, we can write,

$$\begin{aligned} t_n &= (1-d_n) D^{el}_{nn} w_n \\ t_s &= (1-d_s) D^{el}_{ss} w_s, \end{aligned} \tag{1}$$

where t_n is the traction normal to the discontinuity, t_s is the traction tangent to the discontinuity, w_n is the normal jump displacement, w_s is the sliding jump displacement, d_n is the damage variable under normal traction, d_s is the damage variable under shear traction and D^{el}_{nn}, D^{el}_{ss} are the elastic normal and shear stiffness coefficients, respectively.

The limit surface (Fig. 1) is dependent on material strength parameters, namely:

$$f_t = f_t(g_n(\kappa_n)) = g_n(\kappa_n) D^{el}_{nn} \kappa_n, \tag{2}$$

$$c = c(g_s(\kappa_s)) = g_s(\kappa_s) D^{el}_{ss} \kappa_s, \tag{3}$$

where f_t is the tensile strength, which is dependent on a scalar variable κ_n, c is the cohesion, which is dependent on a scalar variable κ_s and g_n and g_s are damage evolution laws under mode-I and mode-II fracture, respectively:

$$g_n(\kappa_n) = 1 - d_n = \frac{f_t}{D^{el}_{nn} \kappa_n}, \quad \text{under mode-I fracture,} \tag{4}$$

$$g_s(\kappa_s) = 1 - d_s = \frac{c}{D^{el}_{ss} \kappa_s}, \quad \text{under mode-II fracture.} \tag{5}$$

For example, if exponential softening is adopted, the following damage evolution laws are obtained:

$$g_n = 1 - d_n = \frac{\kappa_{n0}}{\kappa_n} \exp\left[\frac{-f_{t0}}{G_F}(\kappa_n - \kappa_{n0})\right], \tag{6}$$

$$g_s = 1 - d_s = \frac{\kappa_{s0}}{\kappa_s} \exp\left[\frac{-c_0}{G_F^{II}}(\kappa_s - \kappa_{s0})\right], \tag{7}$$

where G_F and G_F^{II} are the fracture energy and the fracture energy under mode-II fracture, respectively. The scalar variables κ_n and κ_s are such that: $\kappa_n = w_n$ under pure mode-I fracture and $\kappa_s = |w_s|$ under pure mode-II fracture. In Eqs. (6) and (7), $\kappa_{n0} = f_{t0}/D_{nn}^{el}$ and $\kappa_{s0} = c_0/D_{ss}^{el}$, where f_{t0} and c_0 are the initial tensile strength and initial cohesion, respectively (see Fig. 1). For mode-I fracture and mode-II fracture we obtain, respectively,

$$f_t = f_{t0} \exp\left[\frac{-f_{t0}}{G_F}(\kappa_n - \kappa_{n0})\right], \tag{8}$$

$$c = c_0 \exp\left[\frac{-c_0}{G_F^{II}}(\kappa_s - \kappa_{s0})\right]. \tag{9}$$

Mixed-mode fracture is defined if $w_n > 0$, whereas mode-II fracture under compressive states is defined if $w_n = 0 \wedge t_n < 0$. The limit surface in the traction space is defined by two functions: f_1 and f_2, in which f_1 is valid for $t_n \geq 0$ and f_2 is valid under compressive tractions ($t_n < 0$), respectively (see Fig. 1). Function f_1 is given by:

$$f_1 = 0 \Leftrightarrow |t_s| = \frac{f_t tan(\phi) - c}{f_t^2} t_n^2 - tan(\phi) t_n + c, \quad (t_n > 0). \tag{10}$$

For f_2, a modified Mohr–Coulomb surface is adopted:

$$f_2 = 0 \Leftrightarrow \begin{cases} |t_s| = \frac{tan(\phi)}{2t_{n,lim}} t_n^2 - tan(\phi) t_n + c, & \text{if} \quad t_{n,lim} \leq t_n \leq 0 \quad \text{(i)} \\ |t_s| = t_s(t_{n,lim}) = t_{s,max}, & \text{if} \quad t_n < t_{n,lim} \quad \text{(ii)}, \end{cases} \tag{11}$$

In Eqs. (10) to (11), ϕ is the internal friction angle of the discontinuity and in (11) $t_{n,lim}$ is the normal traction corresponding to the maximum shear traction (such that $\partial f_2/\partial t_n = 0$, see Fig. 1). From (10) to (11), it is clear that the transition between functions f_1 and f_2 is continuous, with continuous derivative:

$$\frac{\partial f_1}{\partial t_n}_{|t_n=0} = \frac{\partial f_2}{\partial t_n}_{|t_n=0} = tan(\phi). \tag{12}$$

Damage initiation is defined according to:

$$f_1(f_{t0}, c_0) = 0 \quad \vee \quad f_2(c_0, t_{n,lim}) = 0, \tag{13}$$

where dependence on $t_{n,lim}$ is only relevant for (11). Note that either f_1 or f_2 can be adopted under mixed-mode fracture since it is possible to obtain simultaneously $w_n > 0$ and $t_n < 0$, as shown below. Conversely, only surface f_2 is adopted for mode-II fracture under compression.

Generalisation of the model to take into account dilatancy can be done introducing an *equivalent normal jump*, $w_{n,dil}$:

$$w_{n,dil} = w_n - \tan\psi \ \text{sgn}(w_s) w_s = w_n - \tan\psi |w_s|, \tag{14}$$

in which ψ is the dilatancy angle. The total traction–jump relation becomes:

$$\mathbf{t} = \begin{bmatrix} (1-d_n) D_{nn}^{el} & -sgn(w_s) \tan\psi (1-d_n) D_{nn}^{el} \\ 0 & (1-d_s) D_{ss}^{el} \end{bmatrix} \mathbf{w} \tag{15}$$

Surface f_1 is given by:

$$G\xi_s = (\tan(\phi) - G)\xi_{n,dil}^2 - \tan(\phi)\xi_{n,dil} + G, \tag{16}$$

where $\xi_n = w_n/\kappa_n$, $\xi_s = |w_s|/\kappa_s$,

$$G = \frac{c}{f_t} = \frac{1-d_s}{1-d_n} \frac{D_{ss}^{el}}{D_{nn}^{el}} \frac{\kappa_s}{\kappa_n} = \frac{g_s}{g_n} \frac{D_{ss}^{el}}{D_{nn}^{el}} \rho \tag{17}$$

and $\rho = \kappa_n/\kappa_s$.

Under compression, a distinction between tensile and compressive damage normal variables is made ($d_n^+(\kappa_n), d_n^- = 0$). Surface f_2 is given by:

$$f_2 = 0 = \begin{cases} \kappa_s - |w_s| - \frac{\tan(\phi)\frac{D_{nn}^{el}}{D_{ss}^{el}} w_{n,dil} - \frac{\tan(\phi)}{2t_{n,lim}} \frac{\left(D_{nn}^{el}\right)^2}{D_{ss}^{el}} w_{n,dil}^2}{(1-d_s)}, & \text{if } w_{n,dil} > w_{n,lim} \\ \kappa_s - |w_s| - \frac{\tan(\phi) t_{n,lim}}{2(1-d_s) D_{ss}^{el}}, & \text{otherwise.} \end{cases} \tag{18}$$

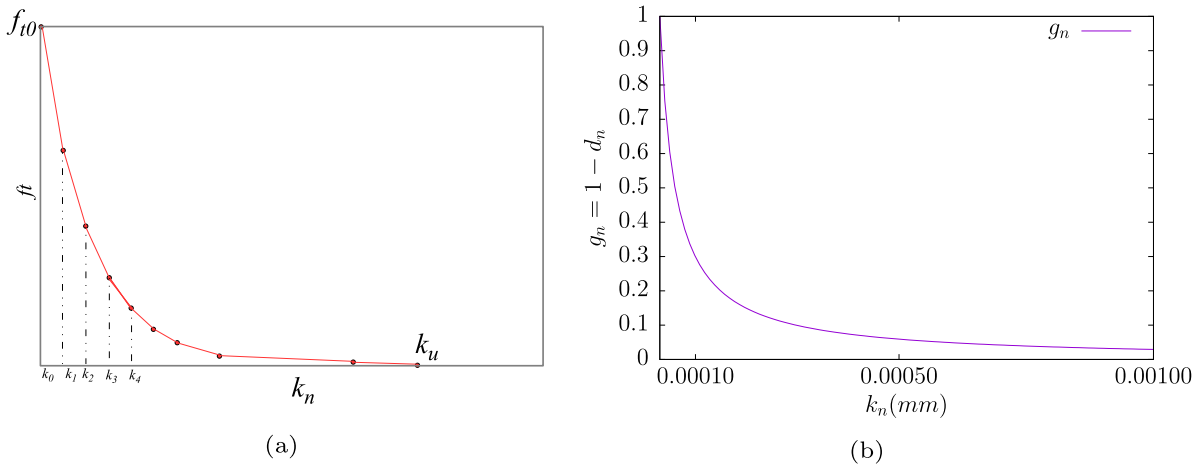

Fig. 2. (a) Multilinear mode-I fracture law, (b) corresponding function $g_n = 1 - d_n$.

In Eqs. (18), $w_{n,lim}$ corresponds to $t_{n,lim}$, $w_{n,lim} = t_{n,lim}/D^{el}_{nn}$.

Note that, in all cases, although both internal variables κ_n, κ_s remain functions of $\mathbf{w}$, i.e. $\kappa_n = \kappa_n(\mathbf{w})$, $\kappa_s = \kappa_s(\mathbf{w})$, they do not vary if the material point remains on the limit surface: $f_1 = 0 \Rightarrow (\dot{\kappa}_n = 0 \wedge \dot{\kappa}_s = 0)$, $f_2 = 0 \Rightarrow \dot{\kappa}_s = 0$. Furthermore, if variables κ_n and κ_s increase, the stress state must remain on the surface:

$$\dot{\kappa}_n > 0 \Rightarrow \dot{f}_1 = 0, \quad \dot{\kappa}_s > 0 \Rightarrow (\dot{f}_1 = 0 \wedge \dot{f}_2 = 0). \tag{19}$$

As a consequence, the Kuhn–Tucker conditions as well as the consistency condition are satisfied:

$$\dot{d}_n \geq 0, \quad \dot{d}_s \geq 0, \quad f \leq 0, \quad \dot{d}_n f = 0, \quad \dot{d}_s f = 0, \quad \dot{d}\dot{f} = 0. \tag{20}$$

3. The incremental approach

The Incremental Approach is a non-iterative approach and was introduced in the works presented in [32–34], with both a continuum hypoelastic model and a discrete crack model. In the work presented in [35], use of a similar procedure was adopted for particle systems.

3.1. Trial step

In the incremental approach, stepwise linear constitutive relations are adopted. The structural response is obtained incrementally and the load factor is adjusted to reach the end of each linear interval. Two possibilities must be distinguished: (i) either the material point lies below the limit surface ($f < 0$) or (ii) the material point lies on the limit surface ($f = 0$). In the former case, the procedure described in Section 4.1 is adopted, with non-zero displacement jumps ($\mathbf{w} \neq \mathbf{0}$). In case (ii), the following two possibilities can occur:

1. $f = 0 \wedge \dot{f} \geq 0$;
2. $f = 0 \wedge \dot{f} < 0$;

In case 1., since the material point already lies on the surface, the new step size factor $\lambda = \lambda^*$ must be found such that a material point on the new surface is reached. It is assumed that mode-I fracture evolution can be defined according to the multilinear relationship depicted in Fig. 2(a), which approximates an exponential law. In Fig. 2(b), the corresponding $g_n = 1 - d_n$ function is shown. The step factor λ^* is such that the *closest* endpoint κ_n^* of each linear branch where the material point lies is reached (see Fig. 2(a)):

$$\lambda^* \Leftarrow \kappa_n^* = \{\kappa_{n,i+1}\}^*. \tag{21}$$

In case 2., unloading should take place. Since in the previous true step the constitutive tensor was updated as the tangent, corresponding to a loading situation, an incompatible material response is obtained which may not lead to an admissible solution. The following procedure is adopted in this case:

i. enforce a null step size
ii. update the stiffness matrix to unloading
iii. check conditions 1. and 2. once more

iv. if the incompatible situation prevails, stop.

A similar procedure applies when the material point reaches the surface with the secant matrix and needs to be updated to the tangent stiffness. In these cases, the numerical test can only proceed by switching to a non-incremental approach, as done in [14,19,36].

3.2. True step

In the true step, two situations may occur:

1. the material point lies below the surface;
2. the material point lies on the surface and it is critical.

In case 1., there is no damage update necessary. In case 2., the new value of $\kappa_n{}^*$ is evaluated and therefore all remaining variables (κ_s, d_n, d_s) can be updated accordingly.

4. The Total Approach

The Total Approach is inspired by firstly, the Sequential Linear Approach introduced by Jan Rots and coworkers [9–13,37] and, secondly, the Lattice Models, introduced in [38,39]. For more detailed information on the use of the Total Approach the reader may also be referred to the works presented in [14,30,36,40–46].

Departing from an equilibrium state, damage is forced to increase at some material point, according to a pre-defined scheme. First, a *trial* step is adopted such that the limit surface is reached at one material point, closest to the surface. Next, the *true* step is performed and the damage is increased at this critical material point.

4.1. Trial step

Consider the limit surface given in (16). At the end of the previous *true* step, new values for $\boldsymbol{\kappa}^*$, ρ^*, $\mathbf{d}^*$ and G^* are enforced through the increase of κ_n. In the next *trial* step, the new total jump displacements are defined as $\mathbf{w} + \lambda d\mathbf{w}$, where λ is a step size factor. Note that $\mathbf{w}$ is usually $\mathbf{0}$, unless an initial stress state is present, such as in [41].

It is required that:

$$f^*(\mathbf{w}^*, \boldsymbol{\kappa}^*, \rho^*, G^*) = 0, \tag{22}$$

with factor λ such that $\mathbf{w}^* = \mathbf{w} + \lambda d\mathbf{w}$. From Eq. (14), we get:

$$\frac{G}{\kappa_s}|w_s + \lambda dw_s| = \frac{(\tan(\phi)-G)(w_{n,dil}+\lambda dw_{n,dil})^2}{\kappa_n^2} - \frac{\tan(\phi)(w_{n,dil}+\lambda dw_{n,dil})}{\kappa_n} + G, \tag{23}$$

which can be solved for λ. A minimum λ value corresponds to the material point closest to the surface, the *critical point*. Due to the absolute value $|w_s + \lambda dw_s|$, and taking into account that, considering dilatancy, this term is also present in $w_{n,dil} + \lambda dw_{n,dil}$,

$$w_{n,dil} + \lambda dw_{n,dil} = w_n + \lambda dw_n - \tan\psi|w_s + \lambda dw_s|, \tag{24}$$

three situations are identified: (i) $w_s \approx 0$, (ii) $w_s dw_s > 0$ and (iii) $(w_s dw_s < 0) \wedge (|w_s| < \lambda|dw_s|)$. The following strategies are adopted [19]:

(i) in case $|w_s| \approx 0$, take $|w_s + \lambda dw_s| = |\lambda dw_s|$ and evaluate λ from (23);
(ii) otherwise, take $|w_s + \lambda dw_s| = |w_s| + \lambda \operatorname{sgn}(w_s) dw_s$ and evaluate λ from (23);
(iii) if $w_s dw_s < 0 \wedge |w_s| < \lambda|dw_s|$, take $\lambda \leq \frac{-w_s}{dw_s}$.

In (iii), the adopted λ value enforces $w_s + \lambda dw_s = 0$, which prevents a change in sign from w_s to $w_s + \lambda dw_s$.

4.2. True step

In the true step, once a critical point is found ($f_1 = 0 \vee f_2 = 0$), the corresponding stiffness is updated. First, damage is increased and this is achieved by enforcing the increase of κ_n by a certain prescribed amount.

Suppose that the mode-I multilinear relationship depicted in Fig. 2(a) is again considered and that κ_n is forced to evolve from $\kappa_{n0} \approx 0$ corresponding to $f_t = f_{t0}$ to κ_u corresponding to $f_t = 0$, in n equally distributed steps, which gives:

$$\kappa_n^* = \kappa_n + \frac{\kappa_u - \kappa_{n0}}{n}. \tag{25}$$

After evaluating κ_n^*, according to the defined damage criterion, it is possible to derive κ_s^*, $d_n^*(\kappa_n^*)$, $d_s^*(\kappa_n^*, \kappa_s^*)$ and to obtain the new total constitutive relation given by:

$$\mathbf{t} = (\mathbf{1} - \mathbf{d}^*) \cdot \mathbf{D}^{el}_{\Gamma_d} \cdot \mathbf{w}. \tag{26}$$

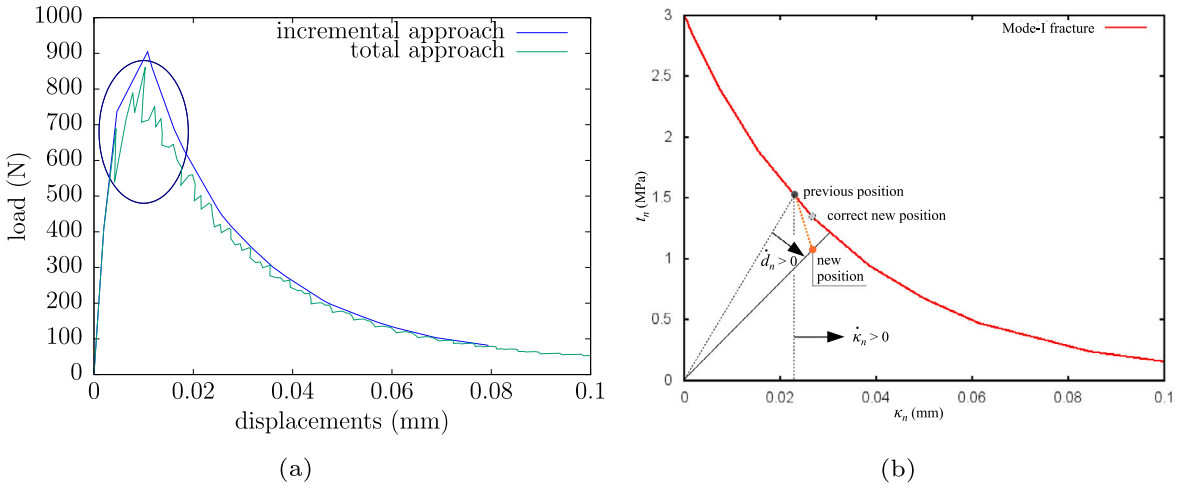

Fig. 3. (a) Abrupt load decay, (b) violation of the consistency condition.

The following increasing function can be adopted:

$$\kappa_n^* = \min\left(\kappa_n + \frac{\kappa_u - \kappa_{n0}}{n}, m\kappa_n\right), \tag{27}$$

where m can take a value which allows for a better approximation of damage near the onset of cracking, for values of κ_n close to κ_{n0} (for instance $m = 2$).

Since κ_n is updated each time the point reaches the surface, its value is prescribed and will remain the actual maximum value until the material point reaches the surface again. Thus, there is no need to evaluate κ_n in each step; this is an advantage from the numerical point of view given the implicit nature of (16).

5. On the Total Approach

In this Section, some considerations on the conventional Total Approach are presented. The main advantage ot the Total Approach is robustness, since a positive definite stiffness matrix is adopted. Thus, results are always obtained and numerical instabilities cannot occur. Moreover, since the response is stepwise elastic, equilibrium is also always satisfied. Some other inherent characteristics and drawbacks are addressed in the following.

5.1. Decay of the load

In the Total Approach, an abrupt decay in the load often occurs. Since the stiffness update is made at one critical point only, the structural response may be significantly below the *true* incremental response due to an incorrect approximation of the global secant stiffness. In some cases, a large number of steps is then needed to bring the global response again close to the correct envelope response. An example of a bending test is shown in Fig. 3(a), in which large load drops are marked by an ellipse.

5.2. Consistency condition

With the Total Approach, the material law is not enforced exactly. As a consequence, the predicted increase of damage can lead to violation of the consistency condition (20). Assume that one material point lies on the limit surface. If this point is not critical in the next step, it will remain below the surface. If damage increases, conversely to (20), we have:

$$\dot{f} < 0 \wedge \dot{d} > 0 \Rightarrow \dot{f}\dot{d} \neq 0. \tag{28}$$

In Fig. 3(b) this situation is depicted for mode-I fracture. In fact, the material point should lie on the new limit surface (softening curve), i.e., on the "correct new position" indicated in the figure for the same increase in κ_n. This gives rise to the 'saw-tooth' response obtained with the SLA and to a sudden decrease of the load described in Section 5.1.

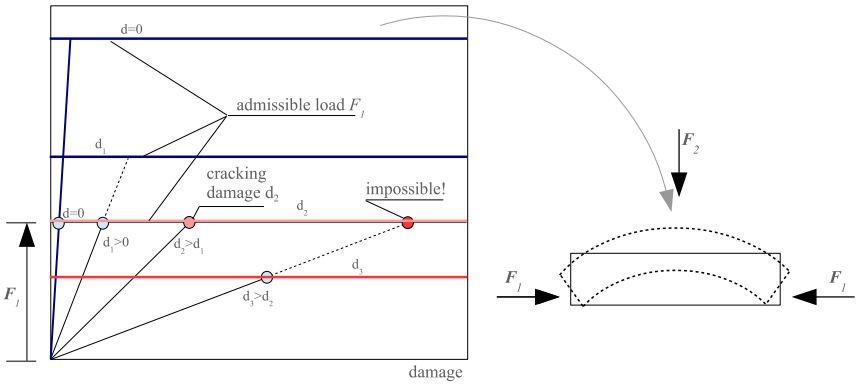

Fig. 4. Non-proportional loading in a pre-stressed beam.

5.3. Non-proportional loading

Implementation of non-proportional loading with a Total Approach has been considered a difficult issue [12,15,17,19,22,47]. Consider a reinforced concrete beam, submitted to three point bending, which is first pre-stressed such that the top surface of the beam is under tensile stress (see Fig. 4). Next, the vertical load is applied until failure occurs. In a conventional Total Approach, the loading corresponding to the pre-stress F_1 is first applied, followed by the vertical load F_2. Since the damage in the beam is increasing under the second loading case, the pre-stress load may lead to cracking starting at the upper surface (d_2 in Fig. 4). In an advanced stage of damage, it might even happen that the beam can no longer withstand the pre-stress and prematurely fail, before the second load is applied (d_3 in Fig. 4). However, in the real test these conditions for the initial pre-stress are never met, since the top surface of the beam will be simultaneously submitted to compressive stresses due to the vertical load.

The solution proposed in [19] is similar to the one adopted in the present work and consists of, as in the real test, enforcing at step m the full load applied in the previous step $m-1$: $F_m = F_1 + \lambda_{m-1} F_2$. In the trial step (see Section 4.1) the value of λ_m is evaluated, which can be either larger or smaller than λ_{m-1}. As a consequence, this issue should no longer be considered a drawback of the Total Approach. Moreover, conversely to the Incremental Approach, the re-evaluation of the stiffness of the whole structure at each step can be interpreted as an advantage: it can be used to properly simulate the effect of damage evolution in time, under constant loading, such as in corrosion.

6. The Total Iterative Approach

It should be emphasised that, in the conventional Total Approach as well as in all non-iterative methods presented in [19], the approximation of the internal variables is not exact, leading to a mismatch regarding the evaluation of the secant stiffness. This feature is taken into account in the Non-iterative Energy based Method (NIEM) presented in [14], but not entirely corrected. In fact, it is shown in [19] that, if the right secant stiffness would have been known, the loading response obtained with these secant methods would lie *exactly* on top of the incremental solution. This mismatch is due to the fact that only one critical material point is considered for damage update.

In the work presented in [22], an incremental iterative procedure is used to mitigate this problem. Nevertheless, since one critical point is still considered, with this method stiffness mismatch is not overcome and saw tooth load–displacement responses are obtained.

In the present work a new model is introduced, designated the Total Iterative Approach. Conversely to the conventional Total Approach, in this new model:

(i) the concept of *Trial step* and *True step* is not used;
(ii) no heuristic stiffness update is performed at the end of each step;
(iii) no single critical material point is defined for damage update;
(iv) damage is updated on several material points simultaneously.

In fact, instead of adopting a pre-defined damage increase in one critical material point, a pre-defined step size increment is enforced, according to a control function C defined below. Due to this new step size, several material points will be lying outside the limit surface. As a consequence, an iterative procedure is adopted such that all points end up lying *on* or *inside* the limit surface.

The most general case of non-proportional loading is considered, in which several external force vectors are applied, $\mathbf{F}_1, \mathbf{F}_2, \dots, \mathbf{F}_n$, which lead to the same number of corresponding stresses and tractions, $\boldsymbol{\sigma}_1, \boldsymbol{\sigma}_2, \dots, \boldsymbol{\sigma}_n$ and $\mathbf{t}_1, \mathbf{t}_2, \dots \mathbf{t}_n$, respectively. Assume that the test is evolving under the second loading case and that a certain load level was attained in step $i-1$: $\mathbf{F}_1 + \lambda_{i-1}\mathbf{F}_2$. In the next step,

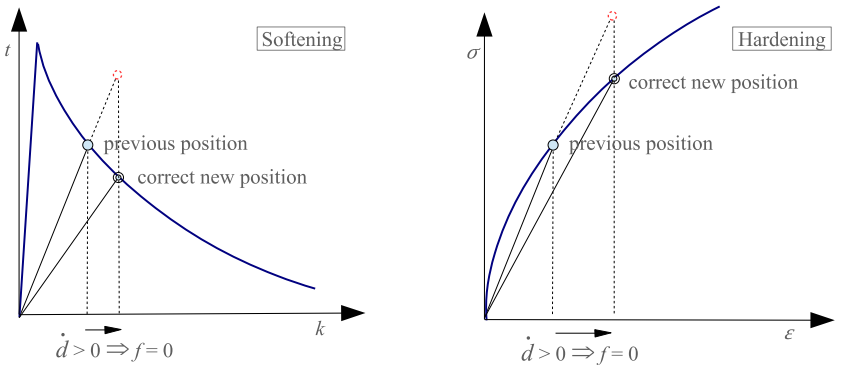

Fig. 5. Uniaxial representation of iteration scheme both for softening and hardening.

the same load level is applied, which should lead to local solutions not lying on the surface ($f > 0$ or $f < 0$). For instance, for mixed-mode fracture, departing from the limit surface given in (10) and assuming $f > 0$, it is possible to write [26,27]:

$$|t_{s1} + \lambda_{i-1} t_{s2}| > \frac{f_t \tan(\phi) - c}{f_t^2} \left(t_{n1} + \lambda_{i-1} t_{n2}\right)^2 - \tan(\phi)(t_{n1} + \lambda_{i-1} t_{n2}) + c. \tag{29}$$

In the conventional Total Approach, a new loading factor λ_i in the *Trial step* is determined such that $f = 0$ in the most critical material point:

$$\left[|t_{s1} + \lambda_i t_{s2}| = \frac{f_t \tan(\phi) - c}{f_t^2} \left(t_{n1} + \lambda_i t_{n2}\right)^2 - \tan(\phi)(t_{n1} + \lambda_i t_{n2}) + c \right]_{crit}, \tag{30}$$

in which the internal variables as well as strength values f_t and c are kept fixed. In the new approach here, an iterative procedure is introduced such that, *for all* points lying outside the surface ($f > 0$), damage is increased until $f \leq 0$ in all these points. For all points lying outside the surface, Eq. (30) becomes:

$$|t_{s1} + \lambda_i^* t_{s2}| = \frac{f_t^* \tan(\phi) - c^*}{f_t^{*2}} \left(t_{n1} + \lambda_i^* t_{n2}\right)^2 - \tan(\phi)(t_{n1} + \lambda_i^* t_{n2}) + c^*, \tag{31}$$

where f_t^* and c^* denote new tensile and cohesion strength values, respectively, corresponding to increasing damage. The same procedure can be applied to further loading if all tractions resulting from previous loading are accumulated in $\mathbf{t}_1$.

In Fig. 5, uniaxial representation of the iterative procedure is depicted at local level, both for softening material and for hardening material. Whenever a material point lies outside the surface ($f > 0$), damage is increased at this point, keeping the kinematic variables κ / ϵ constant, such that the material point lies on the surface. In next iteration, the same procedure is applied to all material points lying outside the surface. Since damage can only increase in each iteration, the iterative procedure stops when $f \leq 0$ everywhere.

In the iterative procedure, step λ_i^* is no longer dependent on the condition $f = 0$ at a single critical point; instead, it will be defined in each iteration, according to a control loading function C. This function can be dependent on the displacements, forces, displacement jumps, as well as internal variables such as damage. Thus, at each step i and each interaction j, step size λ_i^j is defined such that $C = 0$, where $C = C(\mathbf{u}_1 + \lambda_i^j \mathbf{u}_2, \mathbf{F}_1 + \lambda_i^j \mathbf{F}_2, \mathbf{w}_1 + \lambda_i^j \mathbf{w}_2, \mathbf{d}_1 + \lambda_i^j \mathbf{d}_2, \ldots)$. Function C can correspond to a monotonically increasing function of some parameter, taken as an absolute value, similar to the constrained functions used for the arc length method.[1] For instance, in a structure exhibiting hardening behaviour, function C can be given as:

$$C = 0 \Leftrightarrow F_{k,1} + \lambda_i^j F_{k,2} - F_{i-1,k} = \Delta F_{k0}, \tag{32}$$

where k is a chosen degree of freedom (dof) and ΔF_{k0} is a prescribed force increment at this degree of freedom. Since $F_{i-1,k} = F_{1,k} + \lambda_{i-1} F_{k,2}$, Eq. (32) can be written as:

$$C = \lambda_i^j F_{k,2} - (\lambda_{i-1} F_{k,2} + \Delta F_{k0}) = \lambda_i^j F_{k,2} - (F_{i-1,k,2} + \Delta F_{k0}), \tag{33}$$

where $i - 1$ is the previous final step. As a consequence, force F_k increases monotonically by ΔF_{k0} in each step. The larger this increment the larger the number of iterations is expected. However, this is a particular advantage with respect to the conventional Total Approach since, in the latter, there is no control *a priori* of the step size. Moreover, load decay cannot occur using this control function. Note that, since the iterative process starts from the previous equilibrium state *plus* $\Delta\mathbf{F}$, the structure is never evaluated under forces $\mathbf{F}_1$ alone and the issue mentioned in Section 5.3 for non-proportional loading is not addressed.

Some examples of C functions are given below, where, as above, current loading corresponds to $\mathbf{F}_2, \mathbf{u}_2, etc.$:

[1] In fact, this function only needs to be monotonic, but if the absolute value of the control parameter is adopted we get a monotonic increasing function in all cases.

(i) monotonic increase of force at dof k:

$$C = \lambda_i^j F_{k,2} - (\lambda_{i-1} F_{k,2} + \Delta F_{k0}), \tag{34}$$

(ii) monotonic increase of displacement at dof k:

$$C = \lambda_i^j u_{k,2} - (\lambda_{i-1} u_{k,2} + \Delta u_{k0}), \tag{35}$$

(iii) monotonic increase of normal or shear jump displacement w at discontinuity c:

$$C = \lambda_i^j w_{c,2} - (\lambda_{i-1} w_{c,2} + \Delta w_{c0}), \tag{36}$$

(iv) monotonic increase of damage at material point m:

$$C = d_{i,m}^j - (d_{m,i-1} + \Delta d_{m0}), \tag{37}$$

(v) monotonic increase of global displacements:

$$C = \lambda_i^j |\mathbf{u}_2| - (|\mathbf{u}_{i-1,2}| + |\Delta \mathbf{u}_0|), \tag{38}$$

(vi) monotonic increase of the global solution :

$$C = \lambda_i^j \left(\frac{|\Delta \mathbf{u}_2|}{|\Delta \mathbf{u}_{20}|} + \frac{1}{\lambda_0} \right) - 2.0, \tag{39}$$

(vii) monotonic increase of the global displacement jumps:

$$C = \lambda_i^j |\mathbf{w}_2| - (|\mathbf{w}_{i-1,2}| + |\Delta \mathbf{w}_0|). \tag{40}$$

In (38), (39) and (40), $|.|$ represents the norm of the corresponding vector entities $(.)$. In (38), $|\Delta \mathbf{u}_0|$ is the prescribed increment of the displacement norm, in (40), $|\Delta \mathbf{w}_0|$ is the prescribed increment of the displacement jump norm obtained from all or some pre-defined discontinuities. In (39), values $|\Delta \mathbf{u}_{20}|$ and λ_0 are usually taken as the norm of the incremental displacement and the load factor, respectively, obtained at the first step of the current loading case $\mathbf{F}_2$. Although control function (34) is adequate for hardening behaviour only, functions (35) and (38), can also be used for softening behaviour, whereas functions (37), (39) or (40) are general. Function (36) is usually adopted in more critical cases, such as snap-back, in which a monotonic increase of the displacement jump between the two faces of a discontinuity is known to occur.

Thus, the crucial aspect of the iterative process lies on the choice of the control loading function C. This is not a closed issue: definition of function C is and will remain open, allowing to explore new possibilities which lead to a better and swifter approximation of the final solution. For instance, other criteria and corresponding control functions for snap-back will be presented in Section 7.4. A more refined scheme for the increase of damage is also adopted below due to the initial steep functions $g = (1 - d)$ (4) and (5), such as the one shown in Fig. 2(b) corresponding to exponential softening.

7. Numerical examples

In the following, some numerical examples obtained with the Total Iterative Approach are presented. First, comparison with the Total Approach is made, since it is representative of several non-iterative methods. Whenever possible, the results obtained with the Incremental Approach are also shown, which are adopted as reference results.

7.1. Bending

In this Section, examples of a concrete beam under three point bending are presented. These are usual benchmark tests used to assess softening behaviour. Two meshes are used: one rather coarse mesh and another more refined mesh. Both meshes are shown in Figs. 6(a) and 6(b), respectively. In both cases, cracking is modelled with interface elements located at the centre of the beam. The beam is 80 mm wide, 12 mm high and 100 mm thick.[2] The material is concrete ($E = 32$ GPa), with tensile strength $f_{t0} = 3$ MPa, fracture energy $G_F = 0.09$ N/mm and compressive strength $f_c = 27.4$ MPa. In Figs. 7(a) and 7(b), results obtained with the coarse mesh are shown. For clarity, the vertical load and the vertical displacement are displayed as positive values. Hereafter the results obtained with the Incremental Approach (IA) are coloured in blue, the results obtained with the Total Approach (TA) are coloured in green and the results obtained with the Total Iterative Approach (TIA) are in brown. In Fig. 7(a), comparison between the load–displacement results obtained with both the IA and the TA is shown. In Fig. 7(b), comparison between the load–displacement results obtained with both the IA and the TIA is shown. The TIA solution was obtained adopting the control loading function given in (35), where the degree of freedom k corresponds to the vertical displacement under the applied load, at the top of the beam, with $\Delta u_{k0} = -0.002$ mm ($\downarrow$). Thus, in each step, the vertical load displacement is enforced to increase 0.002 mm downwards.

The IA solution was obtained with 21 steps, the TA solution with 368 steps and the TIA solution was obtained with 40 steps, although with iterations. In spite of the fact that the TA solution was obtained with small increments the saw tooth response still

[2] In fact, the thickness is merely an *amplification* factor of the solution since a plane stress state is adopted.

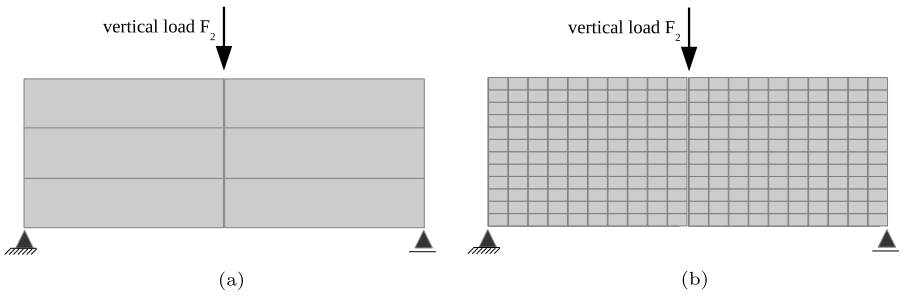

Fig. 6. Three point bending tests: (a) Coarse mesh, (b) refined mesh.

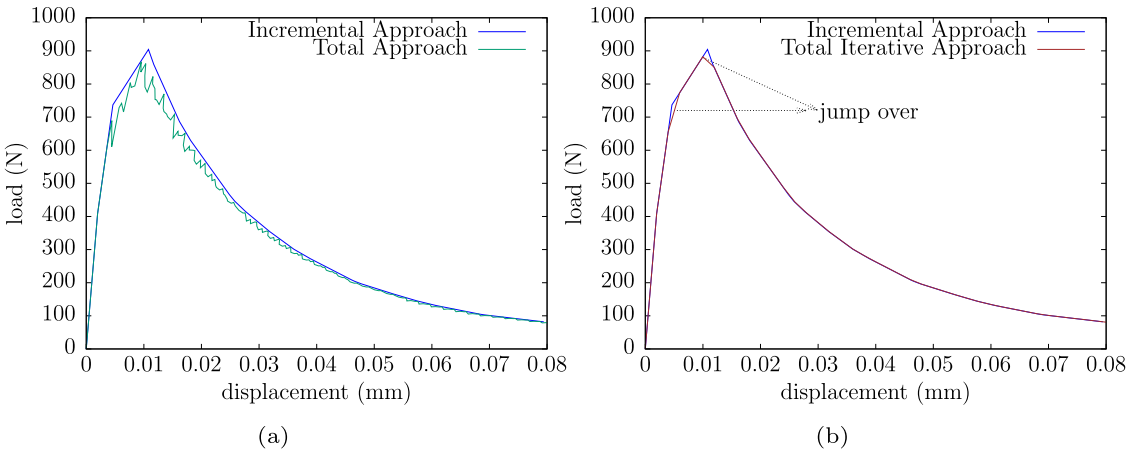

Fig. 7. Bending tests: load–displacement curves obtained with the coarse mesh: (a) IA and the TA, (b) IA and the TIA.

remains obvious. On the other hand, the TIA solution lies on the IA solution. Note that the IA solution was obtained with each step adapted to reach every point of the linearised material law. Conversely, the TIA solution is obtained according to the control function $C = 0$, so the step size is defined differently; in this case, each point of the load–displacement curve is obtained with a constant increment of the vertical loading displacement. This is why, in Fig. 7(b), the TIA solution *jumps over* the IA solution into the next branch twice, although the final position is always on the IA curve (see also Fig. 9(a)). Conversely, the TA solution only lies on the IA solution on the first elastic step.

In Figs. 8(a) and 8(b), results obtained with the refined mesh are presented. In Fig. 8(a), comparison between the load–displacement results obtained with both the IA and the TA is shown. In Fig. 8(b), comparison between the load–displacement results obtained with both the IA and the TIA is shown. Same parameters from the previous test were adopted in the TA and the TIA. The IA solution was obtained with 64 steps, the TA solution with 544 steps and the TIA solution was obtained with 40 steps, although with iterations (0.002 mm $\times$ 40 steps $= 0.08$ mm, using both the coarse mesh and the refined mesh). The same observations from the coarse mesh apply. Note that the high number of steps in the TA must be compared to the total number of steps $\times$ the number of iterations in the TIA, which was 344 in this case. Nevertheless, even if these numbers are similar, the solutions are totally different, with the TIA solution lying on top of the IA solution. Furthermore, it is important to note that both the IA with the TA or with the TIA can be used, as done in [14,19] for the former case, which may lead to an important decrease in the number of iterative steps.

It is interesting to note that, even if the step size increment for the TIA increases significantly, all points of the load–displacement curve still lie on top of the load–displacement curve obtained with the IA. In Fig. 9(a), an increment of -0.01 mm ($\downarrow$) was adopted for Δu_{k0}, leading to only 9 steps with 103 iterations (the first step is enforced such that the tensile strength is obtained at the crack mouth and does not depend on Δu_{k0}). In Fig. 9(b), only the points of the same load–displacement curve are shown, which all lie on top of the IA solution. From these figures it is clear that a large number of steps is not necessary to properly approximate the solution with the TIA, although a variable increment Δu_{k0} may be preferable, as discussed in the following. However, a small number of steps gives rise to a non-conservative evaluation of the energy dissipation as can be seen in Fig. 9(a).

7.2. Prestress

As mentioned in Section 5.3, prestress consists of an example of non-proportional loading. The same concrete beam used in the previous Section is considered, with the refined mesh presented in Fig. 6(b). First, a horizontal force of $F_1 = -1800$ N ($\leftarrow$),

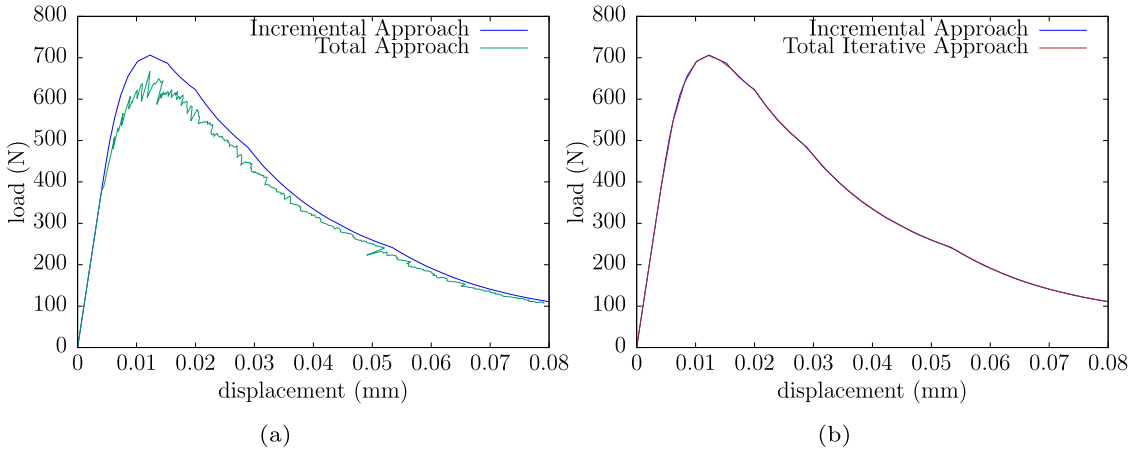

Fig. 8. Bending tests: load–displacement curves obtained with refined mesh: (a) IA and the TA, (b) IA and the TIA.

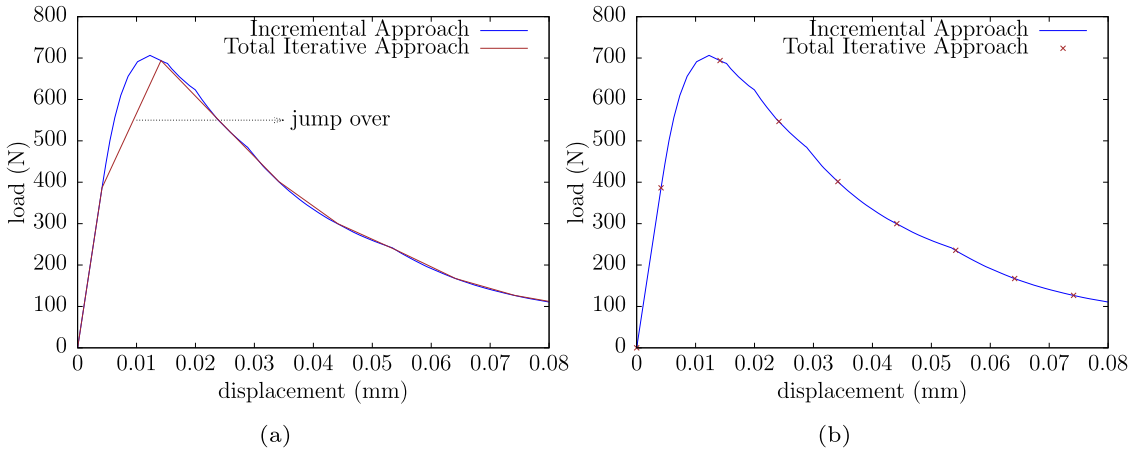

Fig. 9. (a) Bending tests: load–displacement curves with the IA and the TIA, (b) load–displacement points obtained with the TIA on top of the IA solution.

simulating the prestress, is applied at the node adjacent to the right support. Next, a vertical load F_2 is applied until the maximum vertical displacement at the top of the beam reaches -0.08 mm ($\downarrow$).

In Fig. 10(a), comparison between the load–displacement results obtained with both the IA and the TA is shown. In Fig. 10(b), comparison between the load–displacement results obtained with both the IA and the TIA is shown. The prestress force is first applied using the IA in all cases. In the TA, the Improved Non-proportional Analysis introduced in [19] was adopted. In the TIA, the vertical displacement increment adopted in Fig. 10(b) is $\Delta u_{k0} = -0.002$ mm ($\downarrow$). In the load–displacement curves a horizontal negative displacement (upwards) is first obtained with $F_2 = 0$ corresponding to the application of the prestress force F_1. An increase in load capacity from around 700 N (see Section 7.1) to 1500 N is observed, due to the prestress.

Several crack modelling techniques have been used in the literature, namely embedded discontinuity approaches [48–50] as well as the extended finite element method, XFEM [51,52]. In Fig. 11(a), the TIA solution is obtained with the vertical displacement increment of $\Delta u_{k0} = -0.002$ mm ($\downarrow$), using the Discrete Strong Discontinuity Approach (DSDA) [53,54]. Since in this formulation each discontinuity is embedded as if it were an interface, the adopted iterative process is exactly the same as the one adopted for interfaces. In Fig. 11(b), the primary and secondary cracking distribution obtained from the same test is presented. Even with plain concrete, secondary cracks develop, although the major dissipation of energy occurs at the central discontinuity.

7.3. Bond–slip

Bond–slip is an important aspect of the nonlinear reinforced concrete behaviour. A simple example is addressed here, in which reinforcement is modelled with truss elements. The connection between the reinforcement and the concrete is modelled with interface elements with initial zero thickness. The material law adopted for bond–slip exhibits softening with $G_F^{II} = 47$ N/mm. In the TIA, a constant increment of the horizontal displacement of the right edge of the bar is enforced (35), with $\Delta u_{k0} = 0.1$ mm. In

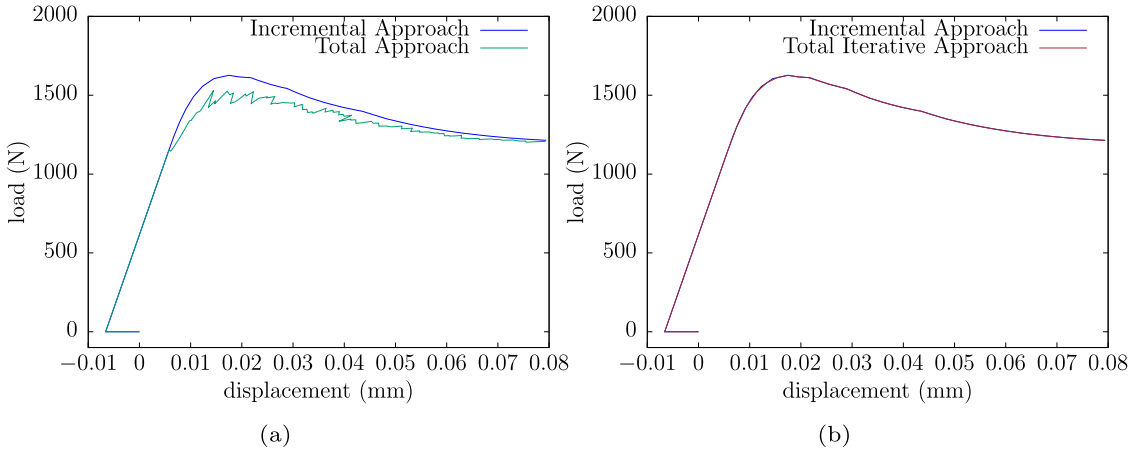

Fig. 10. Prestress tests: load–displacement curves obtained with: (a) IA and the TA, (b) IA and the TIA.

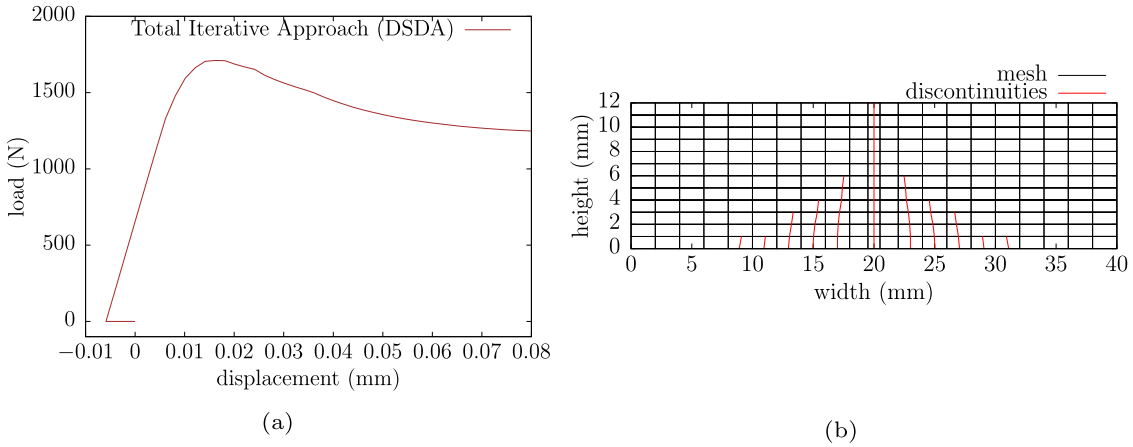

Fig. 11. (a) Prestress tests: load–displacement curve obtained with the TIA using the DSDA, (b) primary and secondary cracking distribution obtained with the DSDA.

Fig. 12(a), the load displacement curves obtained with the IA and the TA are shown, whereas in Fig. 12(b), the load displacement curves obtained with the IA and the TIA are presented

7.4. Snap-back

Snap-back refers to an unstable structural response, difficult to obtain either experimentally or numerically. Since both displacement and load decrease after the peak, neither displacement control nor load control can be used. Based on experimental evidence, it is possible in particular cases to enforce the monotonic increase of the displacement jump at a certain discontinuity location, often the crack mouth opening displacement (CMOD) or the crack mouth sliding displacement (CMSD). With the TIA, this corresponds to the control function C defined in (36).

The first test is a three point bending test with the refined mesh presented in Fig. 6(b), but with a fracture energy much smaller ($G_F = 0.0014$ N/mm), in order to enforce snap-back of the global solution. Exponential softening (6) is adopted in both the TA and the TIA, whereas a corresponding multilinear law is adopted incrementally. In this test, a very sharp peak is obtained, where large load increments/ decrements and small displacement increments/ decrements are exhibited. A constant increment of the CMOD (constant Δw_{n0}), would lead to a rough estimation of the peak load. If small increments were adopted to better approximate the solution near the peak, a large number of unnecessary steps would be used to approximate the much softer post-peak region of the load–displacement response. A non uniform increment w_n can be adopted in this case, such that small increments are enforced near the peak and larger increments are adopted in the post-peak region. Here, the adopted jump increment is made to vary between $\Delta w_0 = 5 \times 10^{-6}$ mm and $\Delta w_0 = 5 \times 10^{-4}$ mm (the maximum value adopted in the multilinear law is $w_u = 1.8 \times 10^{-3}$ mm).

In Fig. 13(a), the load–displacement curves obtained with the IA and the TA are shown. In Fig. 13(b), the load–displacement curves obtained with the IA and the TIA are presented. The displacement scale is enlarged to allow for an easier comparison between the solutions (the maximum displacement shown is very small: 0.01 mm).

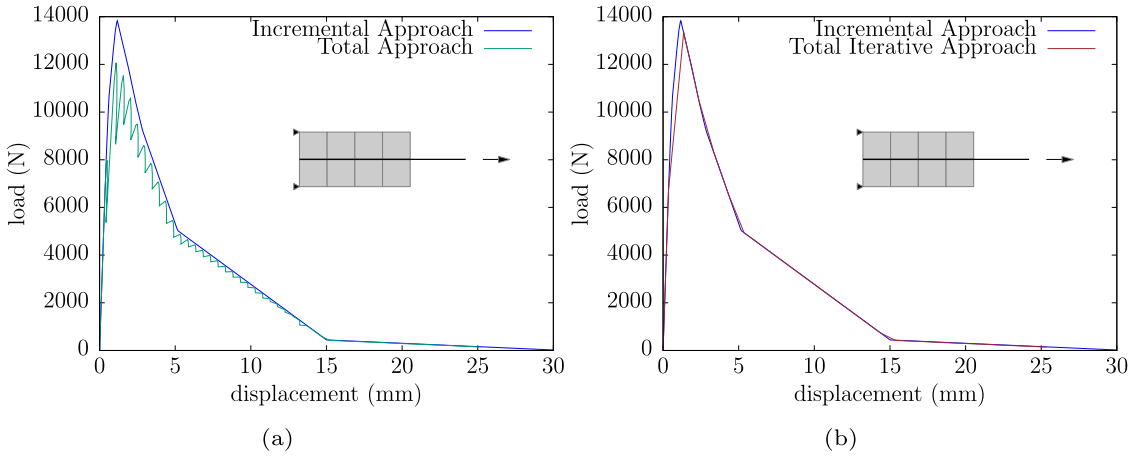

Fig. 12. Bond–slip tests: load–displacement curves obtained with: (a) IA and the TA, (b) IA and the TIA.

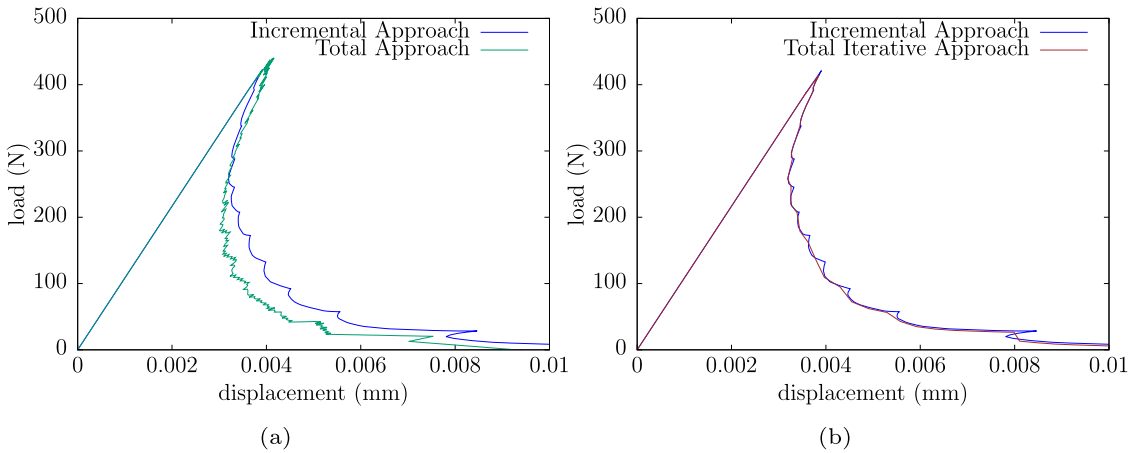

Fig. 13. Snap-back bending tests: load–displacement curves obtained with: (a) IA and the TA, (b) IA and the TIA.

Note that, conversely to the IA, where bifurcations occur and some control of the solution must be given, snap-back is relatively simple to obtain with the TA. In fact, there are no bifurcations in the Total Approach, only stepwise elastic solutions. Moreover, the smaller the fracture energy - or, equivalently, the larger the dimensions of the structure, the smaller the number of material points lying on the surface, i.e., the solution tends to be controlled by one critical point in each step, which is the underlying assumption of the SLA. Thus, simply by increasing the damage at some critical point, it is possible to get a solution. With the TIA, definition of control function C is a central aspect. As with the IA, there is no *magic formula*: the user must know which function should be adopted in each case. In [7], it is found that the possibility of convergence increases if the solution corresponding to the maximum incremental dissipation of energy is adopted. Actually, the solution obtained with the IA is the same using this dissipation energy criterion.

The second test is academic and consists of the modelling of a severe snap-back behaviour in a cantilever beam shown in Fig. 14. Dimensions are: width = 50 mm, height = 100 mm, thickness = 1 mm, fracture energy $G_F = 0.001$ N/mm and a steep linear softening law is adopted. The IA solution is obtained by adopting the energy criterion. In this case, snap-back is so severe that one single material point lies on the surface in each step, which corresponds exactly to the assumption made in the Total Approach. Thus, in this case the TA solution lies on top of the IA solution. The TIA solution is obtained with two new control functions:

1. in the first case, the displacement jump is increased in each active fictitious crack[3] such that a new point in the linearised material law is reached. A fictitious crack is defined as active if it is dissipating energy, which occurs after reaching the material tensile strength and before reaching the last point in the material law, beyond which the local stiffness becomes null

[3] Definition of fictitious crack is given in [55], and refers to the pre-crack stage, in which dissipation of energy occurs.

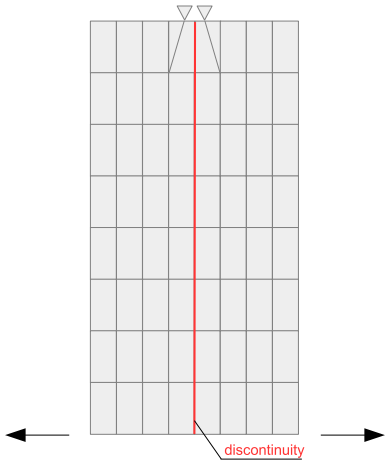

Fig. 14. Snap-back tests: double-cantilever beam, boundary conditions and mesh.

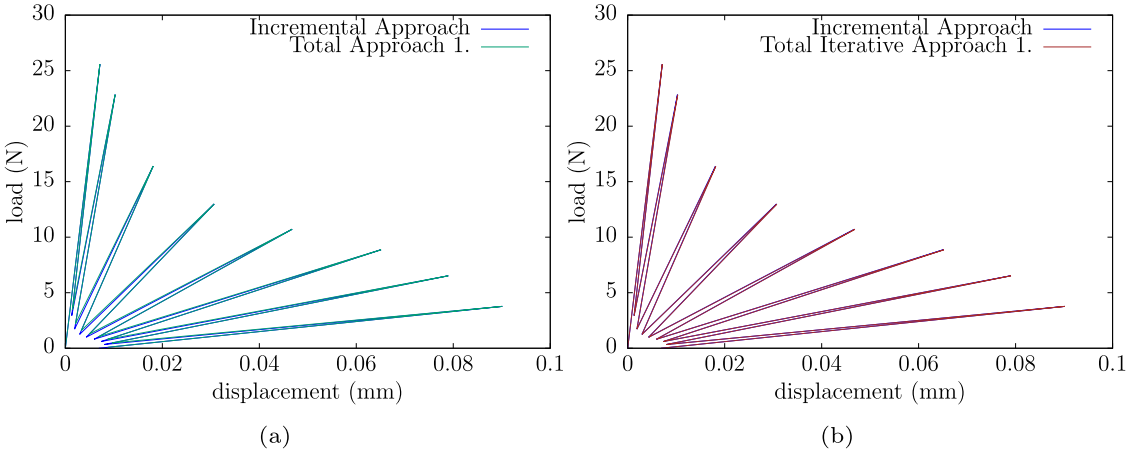

Fig. 15. Snap-back cantilever tests with linear softening: load–displacement curves obtained with: (a) IA and the TA, (b) IA and the TIA (1.)

and a *real* stress free crack is obtained. Function C can be written as:

$$C = \lambda_i^j w_{c,2}^{active} - w_{c,2,m+1}^{active}, \tag{41}$$

where $_{m+1}$ refers to the next point in the material law. Thus, instead of increasing a fixed amount, in each iteration j of step i, the normal jump of the active fictitious crack is enforced to reach the next point in the multilinear law.

2. in the second case, the usual iterative procedure is applied to all material points lying outside the surface, independently of belonging to one active crack or not; however, since the new position on the material law is known *a priori* as in the previous case (.), the local damage is updated accordingly, at the end of each step. In this manner, less points will lie outside the surface, which gives rise to a better approximation of the whole dissipation of energy.

In Fig. 15(a), the load–displacement curves obtained with both the IA and the TA are presented. In Fig. 15(b), the load–displacement curves obtained with both the IA and the TIA with control function (41) are presented. In Fig. 16, the load–displacement curve obtained with the TIA and the control function described in 2 is compared to the load–displacement curve obtained with the IA, using a bilinear softening law. In this figure two deformed cantilever meshes are shown: the first is obtained at one of the lowest points as shown in the figure, corresponding to the threshold of a stress free crack, whereas the second one is obtained at the last peak, corresponding to reaching the tensile strength at the last discontinuity point, also indicated in the figure. Thus, in the cantilever tests presented in Figs. 16, 15(a) and 15(b), the CMOD is always increasing and decreasing during the test, making it impossible to use the same control function (36), adopted in the bending tests presented in Figs. 13(a) and 13(b).

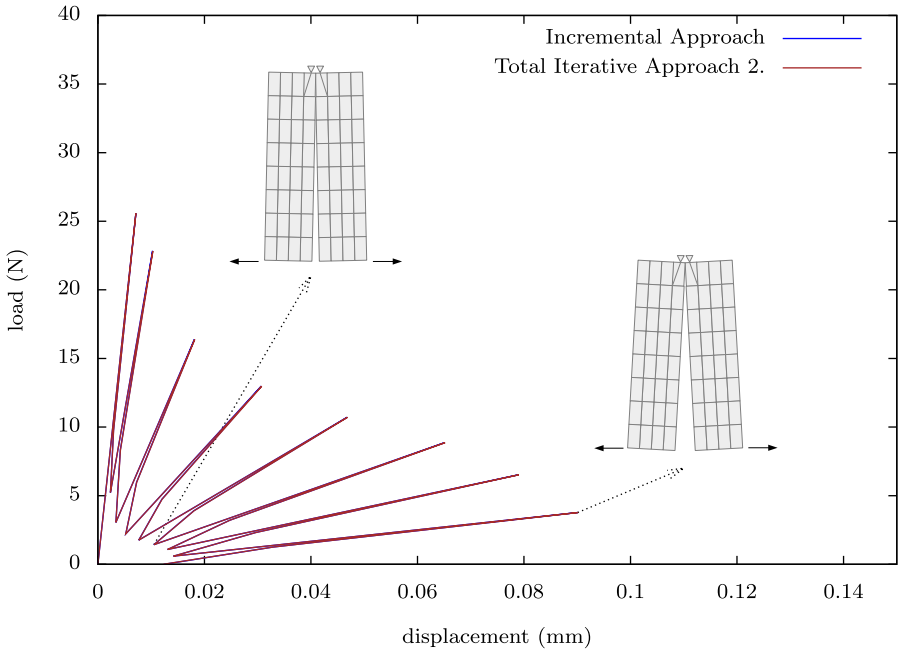

Fig. 16. Snap-back cantilever tests with bilinear softening: load–displacement curves obtained with the IA and the TIA (2.).

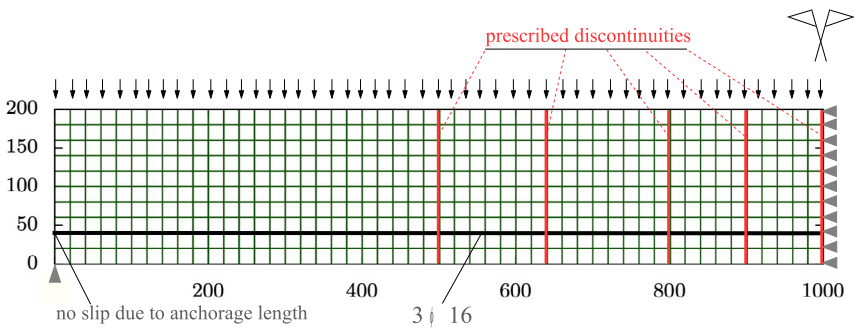

Fig. 17. Reinforced concrete beam: boundary conditions and adopted mesh.

7.5. Reinforced concrete

In this Section a reinforced concrete beam is analysed. The beam is simply supported and is 2 *metres* long, 20 cm high and 30 cm thick. In Fig. 17 half of the beam is represented due to symmetry. The load is distributed on all top nodes of the beam in order to promote a more diffuse cracking distribution. Concrete exhibits the same properties as in Section 7.1, with compressive behaviour modelled as elasto-plastic. The beam is reinforced with 3 bars of 16 mm ($3\phi16$) of steel S400 ($f_{yk} = 400$ MPa), modelled as elastic-perfectly plastic. The bond–slip relationship adopted is given in Table 1, where w_s is the slip between concrete and steel and t_s is the corresponding bond stress.

Five vertical prescribed cracks are defined across half of the length of the specimen in order to allow for multiple cracking, as a consequence of the tension-stiffening effect. The steel bar is located at 40 mm from the bottom surface and is modelled using truss elements. Interface elements are adopted to model the bond–slip behaviour with a dummy normal stiffness. The connection between the left edge of the bar and the concrete is very stiff in order to simulate the effect of the anchorage length. At the central line and due to the symmetry boundary conditions, a fictitious crack is prescribed with a fracture energy equal to half the material fracture energy ($G_{F,sym} = 0.05$ N/mm instead of $G_F = 0.1$ N/mm).

The major issue in this example is crack localisation, which is captured with the Total Iterative Approach using four C functions:

1. enforcing monotonic increase of the vertical displacement at midspan (35),
2. enforcing the monotonic increase of the vertical force at midspan (34),
3. enforcing the monotonic increase of the CMOD of the main discontinuity (36) and

Table 1
Multilinear mode-II fracture relationship adopted for bond–slip.

w_s (mm)	t_s (MPa)
0.20	6.371
0.617	8.749
1.5	7.397
2.0	6.547
2.5	5.791
5.0	3.136
15.0	0.270
30.0	0.000

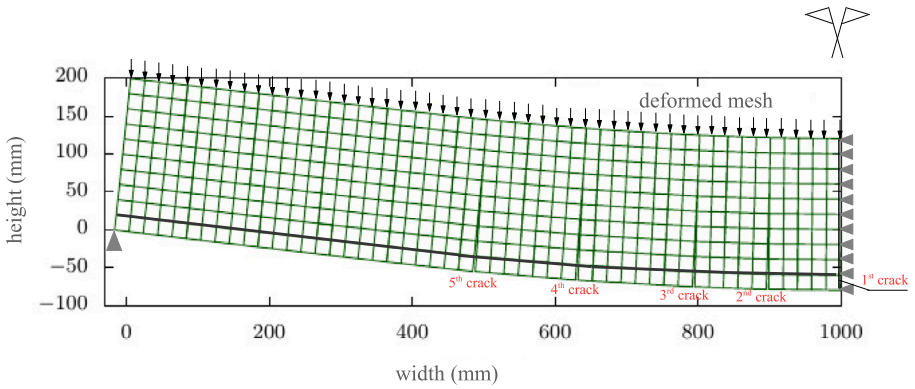

Fig. 18. Reinforced concrete test: deformed mesh with localised cracks at the end of the test (amplification displacement factor = 10).

4. enforcing the monotonic increase of the global solution (39).

The displacement control solution was obtained with a small displacement increment, $\Delta u_{20} = -0.01$ mm (↓), and is taken as the reference solution which is compared to the others. In Fig. 18, the corresponding deformed mesh is shown. In Fig. 19, the load–displacement curves obtained with displacement control and force control are presented. In Fig. 20, the load–displacement curves obtained with displacement control and CMOD control are presented. In Fig. 22, the load–displacement curves obtained with displacement control and global solution control are presented.

In this test, the tensile strength of concrete (3 MPa) is first reached at the central fictitious crack, at the symmetry line. Next, fictitious cracks close to the central line also reach the tensile strength and start to propagate and dissipate energy. In the first steps, 4 fictitious cracks are developing simultaneously, the central crack and the three closest ones. Then localisation starts, and effective propagation of the five discontinuities continues.

Each load drop in the reference load–displacement curve corresponds to crack localisation at some prescribed discontinuity, which occurs simultaneously with unloading of the other fictitious cracks. Counting the discontinuities starting from the symmetry line we obtain (see Figs. 18 and 19):

(i) the first drop is due to localisation of the 2nd discontinuity,
(ii) the second drop is due to the 4th discontinuity,
(iii) the third drop is due to the 5th discontinuity,
(iv) the fourth drop is due to the 3rd discontinuity and
(v) the last drop on the plateau is due to the 1st discontinuity which finally reopens to a full stress free crack.

In this case it was not possible to obtain the whole solution with the Incremental Approach. Note that no iterative procedure is adopted in the IA as detailed in Section 3. A partial incremental solution is shown in Fig. 19, where it can be seen that divergence takes place when crack localisation occurs at the 4th discontinuity (second peak value).

It is interesting to see that, with force control (2.), *snap-through* occurs to points in the curve in which the load is again increasing. Furthermore, the solution stops before localisation at the 1st discontinuity occurs, since the force cannot increase anymore.

The third solution (3.) is obtained by enforcing the monotonically increase of the CMOD at the 2nd discontinuity, defined as the main crack after running solution 1. In this test, crack localisation is not captured step-wise. Note that, although a progressive increase of the CMOD is enforced at each step as shown in Fig. 21, a *snap-through* is also obtained at each load drop in the load–displacement curve. This is due to the fact that, when crack localisation occurs at the other discontinuities, a decrease of the CMOD of the control (2nd) crack would be obtained, which is not allowed in this test. These oscillations in the CMOD happen already in the stress free stage, and are captured with the reference solution. This is why no solution could be obtained with the IA using

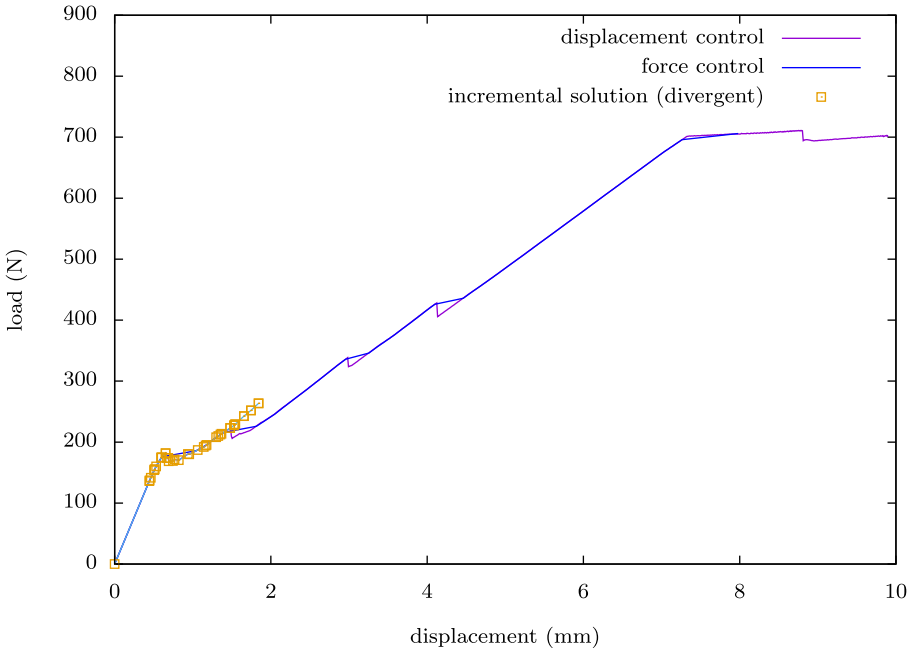

Fig. 19. Reinforced concrete tests: load–displacement curves obtained with the TIA with displacement control and force control; partial IA solution.

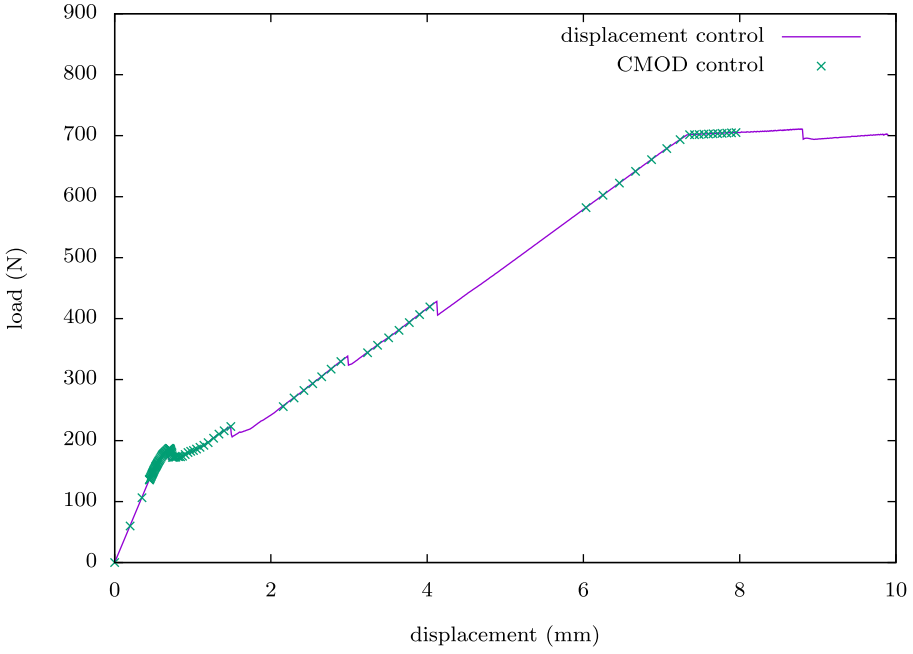

Fig. 20. Reinforced concrete tests: load–displacement curves obtained with the TIA with displacement control and CMOD control.

CMOD control, since it does not increase monotonically. However, with the TIA, the problem is overcome and a next point is always obtained on the curve.

Finally, from Fig. 22 it can be seen that the global solution (4.) is obtained with a small number of steps although it still lies on top of the reference solution.

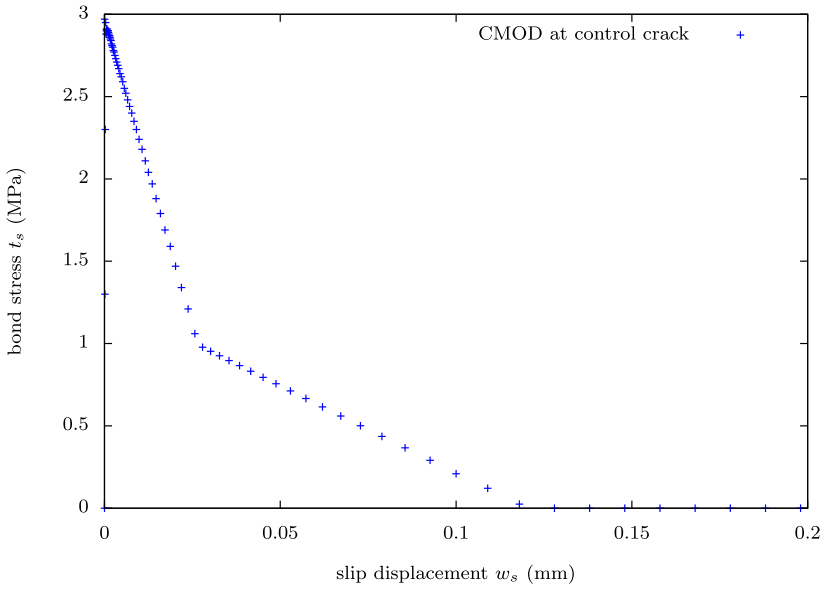

Fig. 21. Reinforced concrete tests: bond–slip curve obtained at 2th crack with CMOD test.

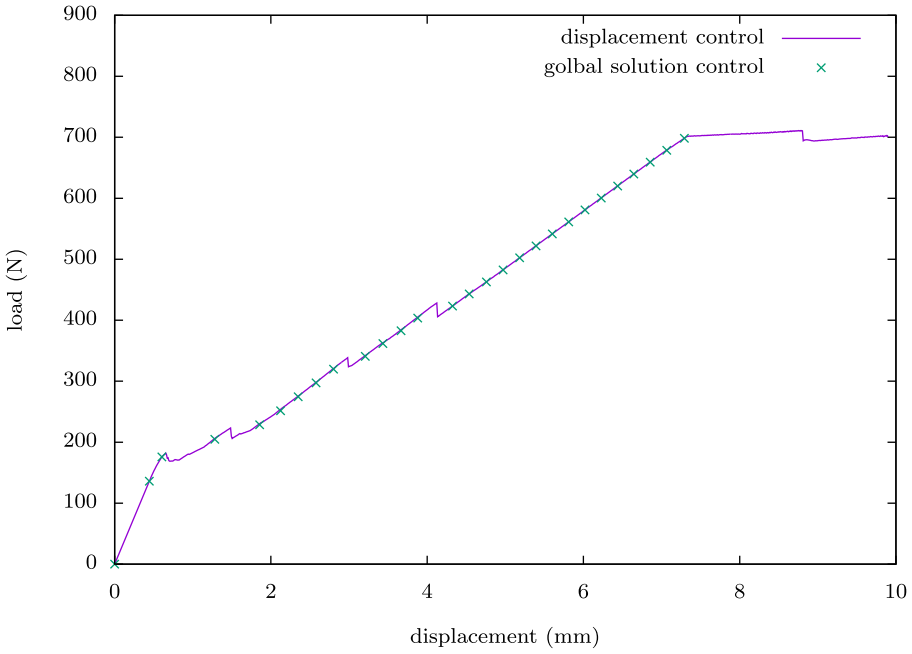

Fig. 22. Reinforced concrete tests: load–displacement curves obtained with the TIA with displacement control and global control solution.

Thus, in this Section it is shown that localisation, a proper sequence of propagating and closing cracks, is difficult to capture even in a relatively simple model as the one presented here. A limited number of cracks is allowed in order to better illustrate the crack localisation phenomenon. In more realistic cases, where cracking is more diffuse, difficult convergence behaviour with traditional iterative algorithms may arise. This is why more robust alternative procedures are needed, such as the TIA.

8. Final remarks

In this manuscript a new Total Iterative Approach is introduced to solve structural problems involving softening materials. The total secant formulation is known to be robust, allowing to overcome critical bifurcation problems. However, in conventional

total approaches such as the ones based on the Sequentially Linear Approach, the Non-Iterative Energy Based Method, the Secant-Incremental Approach, etc., the secant stiffness is updated heuristically in a single material point, leading to problems described in Section 5, namely abrupt load decay and violation of the consistency condition. It is shown in [19] that this is due to an incorrect stiffness update or stiffness mismatch. In fact, incrementally, several points lie simultaneously on the limit surface. All these points must obey the material law, in particular the Kuhn–Tucker conditions, i.e., if the material point lies on the surface and damage increases then the material point should remain on the surface.

Departing from an equilibrium state in an incremental analysis and assuming that unloading is defined according to conventional damage, the *correct* secant stiffness would be obtained upon unloading. In the Total Iterative Approach, internal variables corresponding to these damage states are searched iteratively. This is done by enforcing a control loading function C which, conversely to the Total Approach, locally may push some material points outside the limit surface. The iterative process is defined by increasing damage at these points, such that: (i) function $C = 0$ and (ii) the consistency condition is fulfilled.

In Section 6, the new iterative method is described and definitions of the control loading function C are given. In Section 7, examples are obtained and compared to the TA and to the IA. It is verified that:

i. for all examples presented, the TIA solution lies on top of the IA solution, except in Section 7.5 where the whole incremental solution could not be attained for the IA;
ii. use of large global steps can be adopted with the TIA to approximate the solution;
iii. conversely to the Total Approach, the control loading function allows the enforcement of the step size; thus, at the end of each step, a certain value of displacement, force, displacement jump, etc., is automatically reached;
iv. the most important aspect of the TIA is the control loading function which drives the iterative process;
v. similar to the incremental analysis, this function may have to be adapted to the problem at hand, as in the case of snap-back behaviour 7.4 although, in usual cases, either force control or displacement control can be adopted;
vi. convergence of the iterative process implemented in the Total Iterative Approach is always obtained: since damage can only increase in each material point, the algorithm always provides a solution, where all points lie either *on* or *under* the limit surface.

Finally, it is shown that the Total Iterative Approach is a new model where accuracy and robustness perfectly go hand in hand. As such, the TIA should be considered a powerful tool to solve structures with quasi-brittle materials. Proportional and non-proportional loading examples, bond–slip problems, use of embedded discontinuities such as the DSDA, snap-back behaviour and reinforced concrete, were all properly tackled with this method.

CRediT authorship contribution statement

J. Alfaiate: Writing – original draft, Software, Conceptualization. **L.J. Sluys:** Writing – review & editing, Methodology, Conceptualization.

Declaration of competing interest

The authors declare that they have no known competing financial interests or personal relationships that could have appeared to influence the work reported in this paper.

Data availability

Data will be made available on request.

References

[1] De Borst R, Mulhaus H-B. Continuum models for discontinuous media. In: van Mier JGM, Rots JG, Bakker A, editors. International RILEM/ESIS conference on fracture processes in concrete, rock and ceramics, vol. 2. Noordwijk, The Netherlands: E & FN SPON; 1991, p. 601–18.
[2] De Borst R, Sluys LJ. Localization in a cosserat continuum under static and dynamic loading conditions. Comput Methods Appl Mech Engrg 1991;90(1–3):805–27.
[3] de Borst R. Fracture in quasi-brittle materials: A review of continuum damage-based approaches. Eng Fract Mech 2002;69(2):95–112.
[4] Benallal A, Berstad T, Borvik T, Hoopperstad OS. Uniqueness, loss of ellipticity and localization for the time-discretized, rate-dependent boundary value problem with softening. Internat J Numer Methods Engrg 2010;84(7):864–82.
[5] Crisfield MA. Non-linear finite element analysis of solids and structures, volume 1: essentials. England: John Wiley and Sons; 1991.
[6] Crisfield MA. Non-linear finite element analysis of solids and structures, volume 2: advanced topics. England: John Wiley and Sons; 1997.
[7] Gutiérrez MA. Energy release control for numerical simulations of failure in quasi-brittle solids. Commun Numer Methods Eng 2004;20(1):19–29.
[8] Verhoosel CV, Remmers JJC, Gutiérrez MA. A dissipation-based arc-length method for robust simulation of brittle and ductile failure. Internat J Numer Methods Engrg 2009;77(9):1290–321.
[9] Rots JG. The role of structural modelling in preserving amsterdam architectural city heritage. In: Lourenço Paulo B, Roca Pere, editors. Historical Constructions 2001, Possibilities of Numerical and Experimental Techniques. Guimarães, Portugal, 2001, p. 685–96.
[10] Rots JG. Sequentially linear continuum model for concrete fracture. In: Pijaudier-Cabot G, de Borst R, Mazars J, van Mier JGM, editors. 4th international conference on fracture mechanics of concrete structures. 2001, p. 831–40.
[11] Rots JG, Invernizzi S. Regularized sequentially linear saw-tooth softening model. Int J Numer Anal Methods Geomech 2003;28:821–56.
[12] DeJong MJ, Hendriks MAN, Rots JG. Sequentially linear analysis of fracture under non-proportional loading. Eng Fract Mech 2008;75(18):5042–56.

[13] Rots JG, Belletti B, Invernizzi S. Robust modeling of rc structures with an event- by-event strategy. Eng Fract Mech 2008;75(3–4):590–614.
[14] Costa R, Alfaiate J, Dias da Costa D, Neto P, Sluys LJ. Generalisation of non-iterative methods for the modelling of structures under non-proportional loading. Int J Fract 2013;(21–2):21–38.
[15] Elías J. Generalization of load-unload and force-release sequentially linear methods. Int J Damage Mech 2015;24(2):279–93.
[16] Slobbe Aart Theodoor. Propagation and band width of smeared cracks [Ph.D. thesis], The Netherlands: TUDelft; 2015.
[17] van de Graaf AV. Sequentially linear analysis for simulating brittle failure [Ph.D. thesis], The Netherlands: TUDelft; 2017.
[18] Pari Manimaran. Simulating quasi-brittle failure in structures using sequentially linear methods: Studies on non-proportional loading, constitutive modelling, and computational efficiency. [Ph.D. thesis], The Netherlands: TUDelft; 2020.
[19] Alfaiate J, Sluys LJ. On the use of non-iterative methods in cohesive fracture. Int J Fract 2018;210:167–86.
[20] Vandoren B, De Proft K, Simone A, Sluys LJ. A novel constrained LArge Time INcrement method for modelling quasi-brittle failure. Comput Methods Appl Mech Engrg 2013;265:148–62.
[21] Oliver J, Linero DL, Huespe AE, Manzoli OL. An implicit/explicit integration scheme to increase computability of non-linear material and contact/friction problems. Comput Methods Appl Mech Engrg 2008;197:1865–89.
[22] Chenjie Yu. From sequntially linear analysis to incremental sequentially linear analysis. Robust algorithms for solving the non-linear equations of structures of quasi-brittle material [Ph.D. thesis], The Netherlands: TUDelft; 2019.
[23] Chenjie Yu, Hoogenboom PCJ, Rots JG. Incremental sequentially linear analysis to control failure for quasi-brittle materials and structures including non-proportional loading. Efm 2018;202:332–49.
[24] Chenjie Yu, Hoogenboom PCJ, Rots JG. Extension of incremental sequentially linear analysis to geometrical non-linearity with indirect displacement control. Eng Struct 2021;229:111562.
[25] Alfaiate J, Sluys LJ. Damage and fracture mechanics approaches to mixed-mode discrete fracture with dilatancy. Theor Appl Fract Mech 2019;104(102350). http://dx.doi.org/10.1016/j.tafmec.2019.102350.
[26] Alfaiate J, Sluys LJ. On the modelling of mixed-mode fracture: Part I - localised damage models. Eng Fract Mech 2017;182:157–86a.
[27] Alfaiate J, Sluys LJ. On the modelling of mixed-mode fracture: Part II - Inclusion of dilatancy. Eng Fract Mech 2017;182:245–64b.
[28] Lourenço P, Rots JG. A multi-surface interface model for the analysis of masonry structures. ASCE J Eng Mech 1997;123(7):660–8.
[29] Alfaiate J, Almeida JR. Modelling discrete cracking on masonry walls. Mason Int 2004;17(2):83–93.
[30] Gago AS, Alfaiate J, Lamas A. The effect of the infill in arched structures: Analytical and numerical modelling. Eng Struct 2011;33(5):1450–8.
[31] Pari M, van de Graaf AV, Hendriks Max AN, Rots JG. A multi-surface interface model for sequentially linear methods to analyse masonry structures. Eng Struct 2021;238. http://dx.doi.org/10.1016/j.engstruct.2021.112123.
[32] Alfaiate J, Pires EB, Martins JAC. The influence of the non-linear bulk behaviour of concrete on the 'size dependency of g_f'. In: International RILEM/ESIS conference on fracture processes in concrete, rock and ceramics, vol. 1. 1991, p. 431–40.
[33] Alfaiate J, Pires EB, Martins JAC. A finite element model for the study of crack propagation. In: Aliabadi MH, Cartwright DJ, Nisitani H, editors. 2nd international conference on localised damage. Computational Mechanics Publications and Elsevier Applied Science; 1992, p. 261–82.
[34] Alfaiate J, Pires EB, Martins JAC. A finite element analysis of non-prescribed crack propagation in concrete. Comput Struct 1997;63(1):17–26.
[35] Jirásek M, Bazant ZP. Macroscopic fracture characteristics of random particle systems. Int J Fract 1994;69:201–28.
[36] Costa R, Alfaiate J, Dias da Costa D, Sluys LJ. A non-iterative approach for the modeling of quasi-brittle materials. Int J Fract 2012;178(1–2):281–98.
[37] Slobbe AT, Hendriks MAN, Rots JG. Sequentially linear analysis of shear critical reinforced concrete beams without shear reinforcement. Finite Elem Anal Des 2012;50:108–24.
[38] Schlangen E, van Mier JGM. Experimental and numerical analysis of micromechanisms of fracture of cement-based composites. Cem Concr Compos 1992;14(12):105–18.
[39] Lilliu G, van Mier JGM. 3D lattice type fracture model for concrete. Eng Fract Mech 2003;70(7–8):927–41.
[40] Costa R, Alfaiate J. The numerical analysis of reinforced concrete beams using embedded discontinuities. SDHM, Struct Durab Health Monit 2006;2(1):11–8.
[41] Costa R, Alfaiate J. Concrete beams reinforced with external bonded plates. In: International conference on concrete for structures. 2005.
[42] Graça-e Costa R, Alfaiate J, Dias-da Costa D, Júlio E, Sluys LJ. Numerical modelling of a high-strength prestressed concrete beam using a strong discontinuity approach. In: Barros H, Faria R, Pina C, Ferreira C, editors. International conference on recent advances in nonlinear models – structural concrete applications. 2011.
[43] Graça-e Costa R, Alfaiate J, Dias-da Costa D, Sluys LJ. A new non-iterative approach to fracture. In: Owen DRJ, Oñate E, editors. XI international conference on computational plasticity. 2011.
[44] Graça-e Costa R, Alfaiate J, Dias-da Costa D, Sluys LJ. A non-iterative approach for the modelling of quasi-brittle materials. In: Oliver J, Jirásek M, Allix O, Moes N, editors. International conference on computational modeling of fracture and failure of materials and structures. 2011.
[45] Graça e Costa R, Alfaiate J, Dias da Costa D, Sluys LJ. Modelling the behaviour of lightweight concrete beams using non-iterative numerical methods. In: Jirásek M, Allix O, Moes N, Oliver X, editors. Third international conference on computational modeling of fracture and failure of materials and structures. 2013.
[46] Graça e Costa R, Alfaiate J, Dias da Costa D, Sluys LJ. Generalization of non-iterative numerical methods for damage-plastic behaviour modelling. In: Mier JGM Van, Ruiz G, Andrade C, Yu RC, Zhand XX, editors. VIII international conference on fracture mechanics of concrete structures. FraMCos-8, Toledo, Spain, 2013.
[47] Hendriks Max AN, Rots Jan G, Pari Manimaran. Non-proportional loading in sequentially linear analysis for 3D stress states. Ijnme 2019;119(6):506–31.
[48] Oliver J. Modelling strong discontinuities in solid mechanics via strain softening constitutive equations. Part 1: Fundamentals. Internat J Numer Methods Engrg 1996;39(21):3575–600.
[49] Alfaiate J, Wells GN, Sluys LJ. On the use of embedded discontinuity elements with crack path continuity for mode-I and mixed-mode fracture. Eng Fract Mech 2002;69(6):661–86.
[50] Zhang Yiming, Zhuang Xiaoying. Cracking elements: A self-propagating strong discontinuity embedded approach for quasi-brittle fracture. Finite Elem Anal Des 144:84–100. http://dx.doi.org/10.1016/j.finel.2017.10.007.
[51] Wells GN, Sluys LJ. A new method for modelling cohesive cracks using finite elements. Internat J Numer Methods Engrg 2001;50(2):2667–82.
[52] Areias PMA, Belytschko T. Analysis of three-dimensional crack initiation and propagation using the extended finite element method. Internat J Numer Methods Engrg 2005;63(5):760–88.
[53] Dias da Costa D, Alfaiate J, Sluys LJ, Júlio E. A discrete strong discontinuity approach. Eng Fract Mech 2009;76:1176–201.
[54] Dias da Costa D, Alfaiate J, Sluys LJ, Júlio E. Towards a generalization of a discrete strong discontinuity approach. Comput Methods Appl Mech Engrg 2009;198(47–48):3681–760.
[55] Hillerborg A, Modeer M, Petersson PE. Analysis of crack formation and crack growth in concrete by means of fracture mechanics and finite elements. Cem Concr Res 1976;6(6):773–82.